Contrib Mineral Petrol (2009) 158:543–561
DOI 10.1007/s00410-009-0396-3

ORIGINAL PAPER

The trace element compositions of S-type granites: evidence for disequilibrium melting and accessory phase entrainment in the source

Arnaud Villaros · Gary Stevens · Jean-François Moyen · Ian S. Buick

Received: 6 October 2008 / Accepted: 25 February 2009 / Published online: 24 March 2009

Abstract Within individual plutons, the trace element concentrations in S-type granites generally increase with maficity (total iron and magnesium content and expressed as atomic Fe + Mg in this study); the degree of variability in trace element concentration also expands markedly with the same parameter. The strongly peraluminous, high-level S-type granites of the Peninsular Pluton (Cape Granite Suite, South Africa) are the product of biotite incongruent melting of a metasedimentary source near the base of the crust. Leucogranites within the suite represent close to pure melts from the anatectic source and more mafic varieties represent mixtures of melt and peritectic garnet and ilmenite. Trace elements such as Rb, Ba, Sr and Eu, that are concentrated in reactant minerals in the melting process, show considerable scatter within the granites. This is interpreted to reflect compositional variation in the source. In contrast, elements such as LREE, Zr and Hf, which are concentrated within refractory accessory phases (zircon and monazite), show well-defined negative correlations with increasing SiO_2 and increase linearly with increasing maficity. This is interpreted to reflect coupled co-entrainment of accessory minerals and peritectic phases to the melt: leucocratic rocks cannot have evolved from the more mafic compositions in the suite by a process of fractional crystallisation because in this case they would have inherited the zircon-saturated character of this hypothetical earlier magma. Trace element behaviour of granites from the Peninsular Pluton has been modelled via both equilibrium and disequilibrium trace element melting. In the disequilibrium case, melts are modelled as leaving the source with variable proportions of entrained peritectic phases and accessory minerals, but before the melt has dissolved any accessory minerals. Thus, the trace element signature of the melt is largely inherited from the reactants in the melting reaction, with no contribution from zircon and monazite dissolution. In the equilibrium case, melt leaves the source with entrained crystals, after reaching zircon and monazite saturation. A significant proportion of the rocks of the Peninsular Pluton have trace element concentrations below those predicted by zircon and monazite saturation. In the case of the most leucocratic rocks all compositions are zircon undersaturated; whilst the majority of the most mafic compositions are zircon oversaturated. However, in both cases, zircon is commonly xenocrystic. Thus, the leucocratic rocks represent close to pure melts, which escaped their sources rapidly enough that some very closely match the trace element disequilibrium melting model applied in this study. Zircon dissolution rates allow the residency time for the melt in the source to be conservatively estimated at less than 500 years.

Keywords S-type granite · Trace element · Partial melting · Geochemical modelling · Accessory phases · Cape Granite Suite

Communicated by T. L. Grove.

Electronic supplementary material The online version of this article (doi:10.1007/s00410-009-0396-3) contains supplementary material, which is available to authorized users.

A. Villaros (✉) · G. Stevens · J.-F. Moyen · I. S. Buick
Department of Geology, Geography and Environmental Studies, Centre for Crustal Petrology, Stellenbosch University, Private Bag X1, Matieland, South Africa
e-mail: arnaud.villaros@gmail.com

Introduction

The relationship between S-type granites and their metasedimentary source rocks was established more than

30 years ago, principally on the basis of the major element compositions of the peraluminous granites of the Lachlan Fold Belt in eastern Australia (Chappell and White 1974; White and Chappell 1977; Chappell 1984). In these rocks, relatively high A/CNK ratios (>1.1), low sodium content (Na_2O <3.2 wt%) and K/Na (molar) ratios in excess of 1, as well as Sr and O isotopic ratios consistent with their derivation from sediments were interpreted to reflect the melting of metasediments (S-type). Few studies have considered the relationship between S-type granites and their source rocks from the point of view of trace element compositions (e.g. Sylvester 1998). Where this approach has been followed, the studies have generally focused on small, near-source granitic bodies, where the anatectic zone can be observed and the trace element composition of the source is known (Sawyer 1991; Watt and Harley 1993; Harris et al. 1995; Bea 1996a; Jung et al. 1998; Johannes et al. 2003). Most trace elements display incompatible behaviour during magmatic processes (Rollinson 1993, p. 106). However, observations in the S-type leucogranites, and their source rocks referred to above, demonstrate that the granites are commonly depleted in REE and other "incompatible" elements such as Zr, Hf and Y, relative to what would be predicted from the source composition (Villaseca et al. 2007). Thus, these lower- to mid-crustal granites are interpreted to record trace element disequilibrium during partial melting that is related to the refractory behaviour of the accessory phases that constitute the dominant trace element reservoir in the source rock (Nabelek and Glascock 1995; Bea 1996a, b; Ayres and Harris 1997; Bhadra et al. 2007; Villaseca et al. 2007): refractory minerals do not participate in the melting reactions and lock the largest part of the REE and HFSE budget in the source rock, such that the melting actually affects only the REE and HFSE-poor portion of the rock.

In contrast to some of the near-source granites discussed above, which may arise through low-temperature water-present melting (e.g. Ayres and Harris 1997), large volume S-type granites intruded at high levels in the crust, or their volcanic equivalents, are generally considered to be the product of fluid-absent melting of biotite-bearing assemblages in aluminous metasediments at temperatures of 850°C or higher (Vielzeuf and Holloway 1988; Patino-Douce and Johnston 1991; Vielzeuf and Montel 1994; Gardien et al. 1995; Clemens et al. 1997; Stevens et al. 1997). These granites commonly display a wide range of compositions from leucogranite to granodiorite (Chappell and White 1974; Chappell and White 1992; Collins and Hobbs 2001; Clemens 2003; Stevens et al. 2007). The trace element compositions of these rocks typically show a similarly wide range. However, trace element variation is coupled to the major element composition of the granites in two inter-related ways. First, for many elements, the scatter in concentration values increases as a function of maficity (Fig. 1). Secondly, most trace elements show a positive correlation with maficity (Fig. 1). This observation is supported by the findings of Elburg (1996), who observed that Zr in S-type granites increases as the granites become

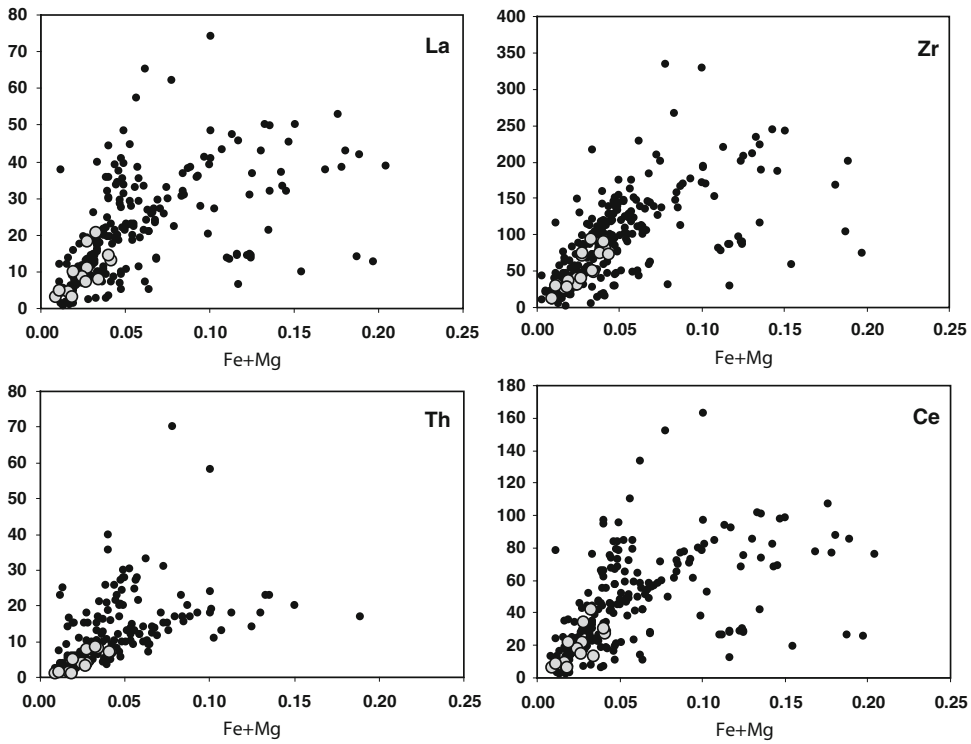

Fig. 1 Atomic Fe + Mg versus trace element concentration (in ppm) diagram. *Black filled circles* represent samples from high level S-type plutons, *grey filled circles* represents the compositions of lower crustal leucogranites. The diagram represents a compilation of 397 published compositions from the following areas: Massif Central, France. (Downes et al. 1990; Williamson et al. 1996; Williamson et al. 1997; Solgadi et al. 2007), Brittany, France (Georget et al. 1986), Himalaya (Ayres and Harris 1997), central Spain (Bea et al. 2006), Lachlan Fold Belt, Australia (LFB Chappell and White 1992), Manitoba, Canada (Goad and Cerny 1981) and the Cape Granite Suite, South Africa (Scheepers 1995)

more mafic and Stevens et al. (2007), who noted a correlation between maficity and total HREE content in S-type granites of the Cape Granite Suite. The near-source leucogranites discussed earlier coincide in trace element composition with the most leucocratic and trace-element poor compositions of the high-level S-type suites.

Given the evidence presented above, it is interesting to consider the potential of trace element behaviour in S-type granites to provide information on the processes in the anatectic source. Several aspects of the granites appear to hold particular promise in this regard. In these rocks, some trace-elements are concentrated in minerals that commonly occur as xenocrysts. Zircon concentrates Zr, Hf and to a lesser degree Y and Yb, whilst xenocrystic monazite, which is reported in rare cases (e.g. Copeland et al. 1988; Parrish 1990) concentrates Ce and La. Other trace elements, such as Rb, Sr, Ba and Eu are concentrated within the minerals that are the major reactants in the melting reactions that produce the granites e.g. Bt + Q + Pl + Sil = Grt + Melt (e.g. Vielzeuf and Montel 1994). Thus, some trace elements may be indicators of the melting reaction, whilst others may trace the degree of dissolution of accessory minerals in the source, as well as the entrainment of these minerals into the magma.

Experimental studies provide useful information on the melt compositions that are produced in the high-temperature fluid-absent anatectic sources of S-type granite magmas. They also provide information on the proportions and compositions of residual and peritectic phases produced during partial melting of likely source compositions. Stevens et al. (2007) used the melt compositions developed in such experiments, in combination with the range of natural rock compositions exhibited by the S-type magmas of the Cape Granite Suite to argue that the major element compositional variations in these granites can be accounted for by variable degrees of entrainment of peritectic phases into the melt. Thus, the general positive correlation between maficity and some trace elements may represent an alternative route to providing information about entrainment processes in the deep crustal source areas to granite magmas. However, the REE and HFSE concentrations of the melts that arise in these sources are not coupled to the stoichiometry of the melting reaction, but rather to the composition of the source and the degree of dissolution and entrainment of accessory minerals. These trace elements therefore present us with an opportunity to evaluate source processes independently from the major element approach. Importantly, as accessory phase dissolution is time dependent, there is possibly potential to constrain the time of residua-melt interaction.

In this study, we test these ideas by constructing a model for the trace element composition of the melts and magmas in the source area of the S-type granites of the Cape Granite Suite in South Africa. These high-level potassic granites appear to have formed through fluid-absent biotite melting at a minimum of 850°C and 10 kbar (Stevens et al. 2007; Villaros et al. 2009). In this model, we consider two alternatives: (1) incongruent melting of biotite to produce a leucogranitic melt and a garnet-dominated peritectic assemblage where there is no equilibration of the melt with accessory phases prior to escaping the source [i.e. trace element disequilibrium melting (TEDM)]. In this case, all of the REE and HFSE remain trapped in accessory minerals; the melt itself is depleted in these elements. The composition of the resultant magmas are a function of the melt composition, the proportion of entrained peritectic assemblage (as per the model of Stevens et al. 2007) and the amounts and compositions of (un-reacted) zircon and monazite entrained to the magma. (2) An identical scenario, but with complete equilibration of the melt with the accessory mineral assemblage [trace element equilibrium melting (TEEM)] prior to segregation. In this case, the monazite and zircon dissolve, the melt is HFSE and REE richer, and the magma compositions are controlled by two parameters only, the melt composition and the entrained peritectic phases. The details of the modelling are presented below.

Geological setting of the Peninsular Pluton

The study focuses on the rocks of the Peninsular Pluton of the Cape Granite Suite of South Africa. The Cape Granite Suite (CGS) contains several plutons; the Peninsular Pluton is one of the least deformed and it contains co-magmatic varieties of granitoids ranging from granodiorite to leucogranite.

The Pan-African Cape Granite Suite was formed during the Saldanian Orogeny, as a consequence of the convergence of Rio de la Plata and Kalahari Cratons during Gondwana assembly (Fig. 2a). The plutons that form the suite intrude the greenschist-facies metasediments of the Malmesbury Group and consist of both S- and I-type granites (Scheepers 1995). The S-type plutons formed between 560 and 530 Ma (Da Silva et al. 2000; Scheepers and Armstrong 2002; Da Silva et al. 2005) and are slightly older than the I-type granites formed between 540 and 520 Ma (Da Silva et al. 2000; Scheepers and Armstrong 2002). The source of the S-type plutons of the CGS is commonly considered to be a higher grade equivalent of the Malmesbury Group metasediments (e.g. Harris et al. 1997) which the granites intrude and which occur as up to amphibolite-facies grade xenoliths within the granites. The S-type CGS consists of four major plutons (Darling, Saldanha, Stellenbosch and Peninsular), located to the south of the NW-SE trending Colenzo Fault (Fig. 2b). Of these plutons, the most southerly body, the Peninsular

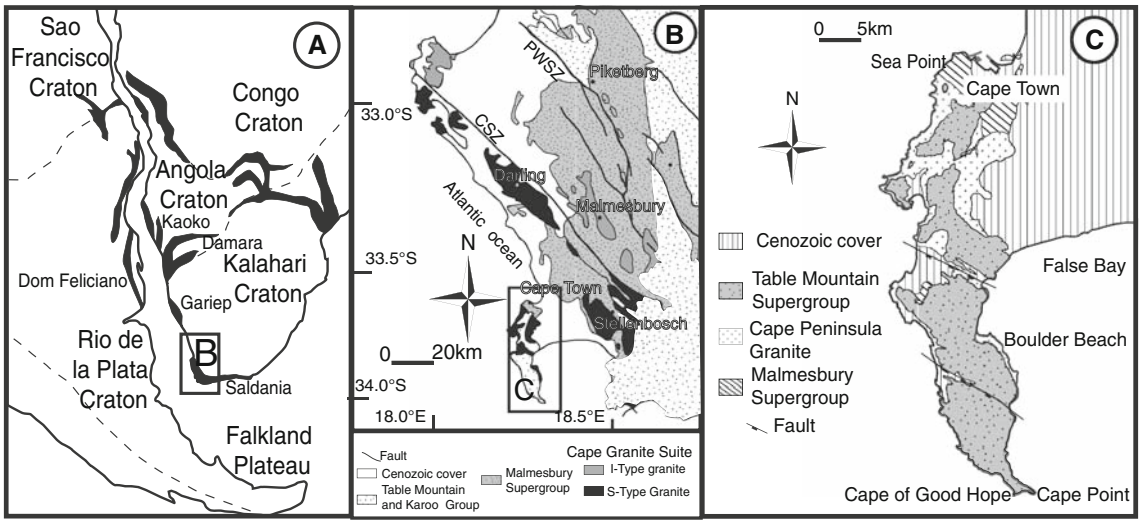

Fig. 2 **a** Palaeogeographic reconstitution of the Saldania orogen at 550 Ma (after Rozendaal et al. 1999). **b** Geological map illustrating the main plutons of the Cape Granite Suite (from Hartnady et al. 1974). **c** Geological map of the Peninsular Granite

Pluton is most suitable for this study in that is essentially undeformed in the solid state, with very little alteration apart from very common pinitisation of cordierite. Furthermore, it contains rocks that record almost the full range of S-type CGS compositions, from leucogranitic to granodioritic. In this sense, apart from having a relatively high-K character, it could be considered to cover the major element compositional range that is typical for S-type granites. The Peninsular Pluton is generally cordierite rich, with rocks containing in excess of 10% cordierite being common. The cordierite is formed from the low-pressure conversion of high-P peritectic garnet entrained in the magma (Stevens et al. 2007; Villaros et al. 2009). Compositional variations are expressed in the proportions of biotite, cordierite, garnet and K-feldspar phenocrysts. Four main facies have been defined within the Peninsular Pluton (Schoch 1975; Schoch et al. 1977); a dominant leucocratic K-feldspar porphyritic granite (Cape Granite) and three minor, more mafic facies: a biotite-rich K-feldspar porphyritic granite (Biotite Porphyritic Granite), a biotite non-porphyritic granite (Biotite Granite) and a granodioritic facies (Cape Granodiorite). The contacts between the facies are generally steep to sub-vertical and diffuse over a 10–20 cm range (Fig. 3a, b) Within the peninsular pluton no sharp contacts have been observed between granite types other than between some magmatic enclaves and their hosts (Fig. 3c, d). There is no systematic layering within the pluton and boundaries between the facies cannot generally be followed for more than a few 10 s of metres. As a general observation, the Cape Granite constitutes the matrix of the Peninsular Pluton, within which the more mafic facies occur as domains elongated in the vertical dimension. The diffuse nature of the contacts between each compositional facies emphasises the fact that the different components of the Peninsular Pluton are co-magmatic.

Stevens et al. (2007) investigated the origin of the major element geochemical diversity in the S-type CGS by using appropriate experimental melt compositions as a guide to the likely natural melt compositions. This study showed that melt compositions developed at temperatures less than 1,000°C from metapelitic and metapsammitic source rocks are always leucogranitic. Thus, this study proposed that the wide range in maficity observed in S-type granites is not the result of the evolution of melts of granodioritic or more mafic composition towards the leucocratic composition by fractionation. Similarly, it is not possible that moderately leucocratic "primitive" melt compositions produced the mafic rocks as crystal cumulates, with the most leucocratic granites then representing the residual liquids, as there is insufficient very leucocratic material to counterbalance the volume of relatively mafic granites. Consequently, Stevens et al. (2007) proposed that the granites left the source as a crystal contaminated magma and that the trends of increasing A/CNK, Ca, Mg# and Ti, and decreasing K and Si, as a function of total Fe + Mg, fit best with the mixing of melt and peritectic minerals (i.e. products of incongruent melting), together with the retention of the remaining un-melted mafic phases ("restites") in the source region. In essence, this means that the granites represent mixtures of peritectic garnet, ilmenite and melt, with the addition of up to 20 wt% of the peritectic products being required as an adjunct in order to match the compositions of the most mafic S-type granites in the suite. Many of the granites proposed to have formed in this way no longer contain garnet due to the replacement of garnet by cordierite and biotite at higher levels within the magmatic system.

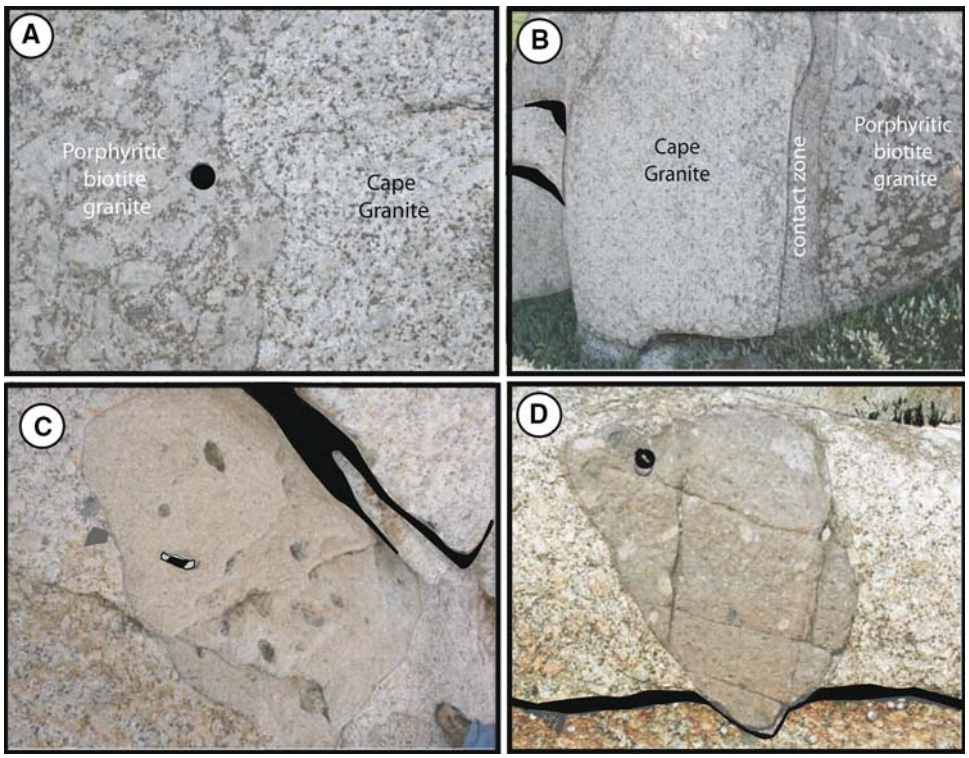

Fig. 3 Field relationships in the Peninsular Pluton. **a**, **b** illustrate the typically diffuse contacts between the different facies. **a** represents a plan view; **b** shows a vertical section through such a contact. The width of the field of view in **b** is about 3 m. **c**, **d** illustrate the sharp contacts displayed by magmatic enclaves as well as the texture of the microgranular magmatic enclave relative to the host Cape Granite

Villaros et al. (2009) have used a pseudosection modelling approach to investigate the origin of garnet in CGS S-type granites that are garnet-bearing, as well as the limits of garnet stability in garnet-free granites that are proposed to have contained garnet near the source. This study has demonstrated that all of the S-type CGS compositions investigated have garnet co-existing with melt at the pressure–temperature conditions of the source. The source conditions are estimated from rare granulite-facies metabasite xenoliths from the Darling batholith (Schoch 1975; Villaros et al. 2009), which record conditions of metamorphism of $P = 10 \pm 2$ kbar and $T = 850 \pm 56$°C. These conditions are consistent with a biotite fluid-absent melting origin for the granite magmas, as proposed by Stevens et al. (2007). The study of Villaros et al. (2009) also demonstrated that garnet preserved within the CGS rocks has equilibrated, through a dissolution-precipitation process, at relatively low pressure within the magma chamber.

Geochemical data

Analytical methods

A suite of samples representative of compositional variation within the Peninsular Pluton was studied. These analysis have been supplemented by the existing database from Scheepers (1995) and Stevens et al. (2007), collectively this represents 43 rock compositions from within the Pluton. Major element compositions have been obtained by XRF analysis on La-free glass beads (Phillip's PW1404w at Stellenbosch University), trace element compositions have been obtained from the same fused beads by applying the method described by Eggins (2003) and analysed using an Agilent 7500ce ICP-MS coupled with a Nd-YAG 223 nm New Wave LASER ablation (LA) system operating at a 12 Hz frequency with a mixed He-Ar carrier gas. Three analyses (each comprising a 30 s blank followed by data collection for 60 s) on each whole rock fused disc were obtained using a 100 μm diameter aperture, and the results averaged. After every three samples (i.e. every 10th analysis) a National Institute of Standards and Technology NIST612 (Pearce et al. 1997) glass bead was analysed as calibration standard, in addition to fused discs of Nim-G (granite) and BhVO-1 (basalt) as secondary standards. Data were collected in time-resolved mode and, were reduced using an Excel calculation spreadsheet using the SiO_2 content measured by XRF as the internal standard. For each element the reproducibility of replicate analyses of the samples, and deviation from the certified values of the secondary standards are better than 10%, and mostly below 5% relative.

Major element data

Major element compositional variation within the Peninsular Pluton is typical of K-rich peraluminous granitoids (Table S1) with SiO_2 content varying from 61.1 to

76.7 wt%; relatively high Al_2O_3 (12.9–17.1 wt%); and highly variable FeOt, MgO and TiO_2 (1.15–10.38, 0.32–3.5 and 0.14–1.91 wt%, respectively). A/CNK varies from 1.14 to 1.64 while X_{Mg} (molecular Mg/(Mg + Fe), all Fe as Fe^{2+}) values lie between 0.31 and 0.41. Figure 4 presents Harker diagrams for FeOt, MgO, CaO, TiO_2, K_2O and A/CNK variation against SiO_2 in the S-type CGS. Experimental melt compositions are plotted for reference. FeOt, MgO, CaO and TiO_2, show coherent trends as a function of SiO_2 content, while variations for K_2O and A/CNK show a larger scatter. The implications of these trends have been discussed in detail by Stevens et al. (2007), who interpreted these trends to reflect melt compositional variation due to a source compositional control, for parameters such as K and Na, and to reflect the entrainment of the ferromagnesian peritectic assemblage to produce the coherent evolution away from leucocratic melt compositions towards the compositions of the more mafic granitoids. The major element composition of the granites is not interrogated further in this study.

Trace element data

The trace element compositions of the granites are variable. In particular, concentrated within monazite (e.g. LREE and Y) and zircon (high field strength elements (HFSE): Zr and Hf) show substantial variation, with maximum concentrations typically about 10 times those of the least enriched rocks. La varies from 10 to 103 ppm; Ce varies from 20 to 216 ppm; Zr values range from 67 to 632 ppm; Hf varies from 2 to 17 ppm and Y varies from 15 to 181 ppm. Some large ion lithophile elements (LILEs) are compatible within phases that are reactants in melting reactions (principally those elements in biotite and plagioclase) also show significant but smaller variations in concentration, a fourfold variation in concentration being

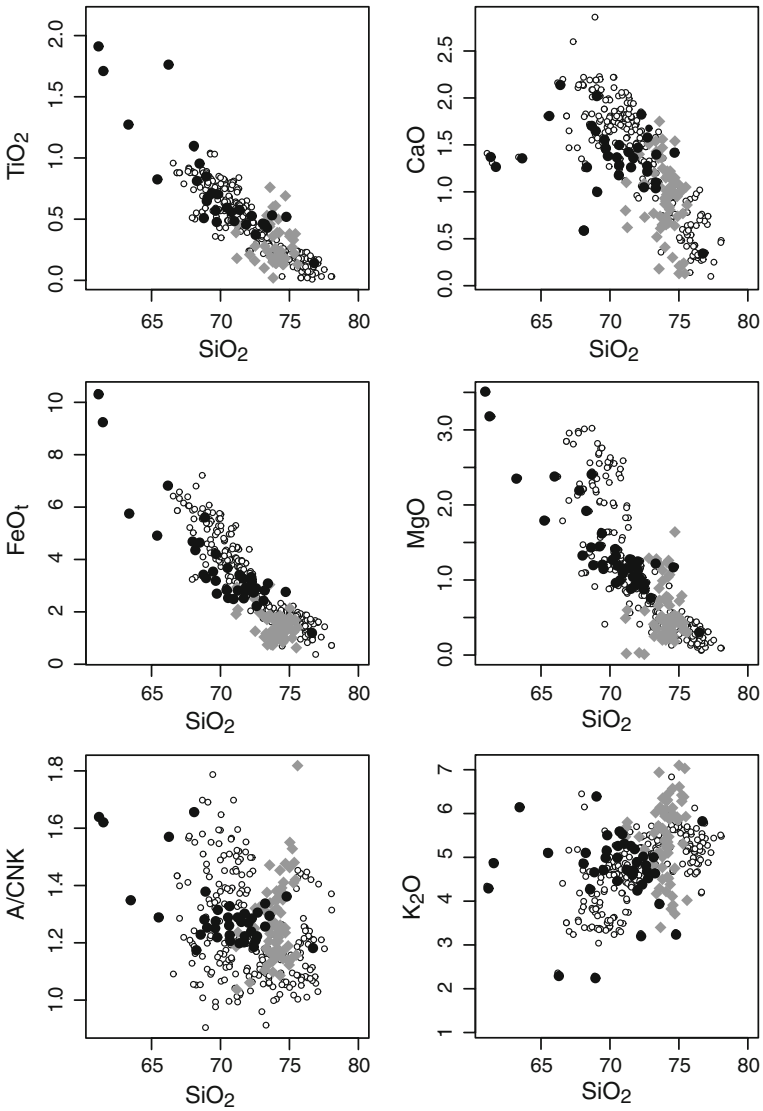

Fig. 4 Harker diagrams displaying compositional variation within the S-type CGS rocks. The black filled circles represent the different the Peninsular Pluton sampled in this study. The *white filled circles* represent a compilation of S-type CGS compositions (*white filled circles* from Scheepers 1995). The *grey diamonds* represent the compositions of experimental melts from both synthetic and natural metasediments at conditions comprised between 8 and 10 kbars and 800–900°C (Patino-Douce and Beard 1995; Stevens et al. 1997; Patino-Douce and Harris 1998; Pickering and Johnston 1998)

typical. For example Rb varies from 127 to 414 ppm, Sr from 32 to 148 ppm, Ba from 52 to 867 ppm and Eu from 0.4 to 1.8 ppm.

Figure 5 show the trends defined by trace elements as a function of maficity. The trends defined by the elements that are concentrated within zircon and monazite (La, Ce, Yb, Zr and Hf) are very similar to the variations displayed by FeOt, MgO, TiO_2 and CaO, i.e. those elements proposed by Stevens et al. (2007) to be strongly controlled by peritectic phase entrainment (garnet and ilmenite). The Fe + Mg range of possible melt compositions plotted on the diagram gives an indication of which rocks may represent those close to pure melts, requiring no Fe + Mg enrichment mechanism to explain the major element chemistry of the rock. Note that in accordance with the observations in near-source granites, these leucogranitic compositions are generally defined by low abundances of the trace element associated with accessory phases relative to the more mafic rocks. In contrast, elements compatible in phases which are reactants during the incongruent melting of biotite (Rb, Ba, Sr and Eu) show a particularly large scatter for the range of rock Fe + Mg values corresponding those of likely melt. They also do not show the clear positive correlation with Fe + Mg defined by the other group. Variations in elements compatible in melting reaction reactant phases can be regarded as a consequence of the concentration of these elements within the reactant phases in the source rock, as well as the proportion of these phases consumed to form the melt or magma, and the degree of equilibration of the melt with residual biotite and feldspar. These elements appear to have peaks in concentration at intermediate (within the dataset) Fe + Mg contents. These are interpreted to represent the magma compositions formed by the highest degrees of biotite and plagioclase consumption relative to the amount of diluting entrained peritectic assemblage. The large degree of scatter at any given Fe + Mg content is interpreted to reflect variations in source mineralogy and trace element composition. These elements are not considered in more detail in this study. In contrast with the above behaviour, trace elements concentrated within monazite (La, Ce, Th) and zircon (Zr, Hf) show a reasonably well defined positive correlation with Fe + Mg.

As the variation of Fe + Mg, Ti, Ca, etc. is interpreted to reflect the degree of peritectic assemblage entrainment (garnet and ilmenite), the good correlation of the monazite and zircon controlled trace elements with these major element compositional parameters suggests the co-entrainment of these accessory phases and the peritectic assemblage. An alternative interpretation might be that the melts which have the greatest capacity to entrain peritectic crystals also have the greatest capacity to dissolve accessory minerals. However, the significant fraction of xenocrystic zircon in the more mafic granitoids argues for co-entrainment. The model developed below sets out to investigate if considerations of zircon and monazite saturation in the melt provide information on the relative contributions of accessory phase dissolution and entrainment to the trace element budget of the rocks.

Modelling trace element behaviour during melting

Zircon and monazite play a negligible role in melting reactions which spawn granite magmas, yet in both the unmelted source and in the crystallised granite, they contain almost all the Zr, Hf, Th, Sm, Nd, Ce and La in the rock. Thus, these elements are related to the major element geochemistry of the rock through processes that control either the dissolution of zircon and monazite in the melt, or the entrainment of these minerals into the magma. As the S-type granite magmas of the CGS are interpreted to represent mixtures of melt and the peritectic assemblage, three possible trace element reservoirs need to be constrained in order to model trace element variations in the granites. These are: the melt; the entrained peritectic assemblage and the entrained accessory minerals. To do this the trace elements composition of the source needs to be defined. This study has used a biotite-quartz-plagioclase schist (BS4) from the proposed source (Malmesbury Group) as a proxy for the granite source composition (Table 1). This rock represents the highest grade non-xenolithic sample of the Malmesbury Group that is available and is derived from a single exposure of homogenous schist. It is assumed that the trace element composition of this rock is not meaningfully different from the trace element composition of the high-grade source of the granite. The trace element composition of BS4 was analysed using the same techniques described for the granites. Zircon in the rock is assumed to have the average composition of 12 inherited zircon cores from the Peninsular Pluton (LA-ICP-MS Villaros, unpublished). This material composition must reflect the actual zircon composition in the source. As sample BS4 is a low-grade metasediment, and monazite is typically not stable at these grades (Kingsbury et al. 1993), the monazite composition used is taken from monazite analysed from a granulite-facies metasediment by Montel (1993) (Table 1). Sample BS4 has Zr and Ce concentrations of 348 and 83 ppm, respectively. Zircon and monazite abundance in the source is calculated by assuming that all Zr and Ce in the source are contained within zircon and monazite, respectively. Thus, the Zr and Ce concentrations measured for BS4 translate to 0.075 wt% zircon and 0.028 wt% monazite in the source. This source composition is used in two forms in modelling the partial melting process. First, with the full complement of trace elements (the TEEM example discussed below), and secondly, with the much reduced trace element budget that would result from all

monazite and zircon being removed from the rock (the trace element disequilibrium example where melting and melt extraction is deemed to be so rapid that accessory phases do not have time to dissolve into the melt and contribute to its trace element composition). The two source compositions are presented in Table 1. The monazite and zircon compositions used in the modelling appear to be appropriate, as the modified source composition has all elements that concentrate strongly into the two minerals at very low values, yet none are strongly negative.

The assemblages that would form in the source during fluid-absent melting are predicted from a pseudosection calculated using PerpleX (Connolly 1990; Connolly and Petrini 2002) for the BS4 composition (Table 1) with 2.5 wt% water (i.e. 6 mol%). This is the amount needed to just fluid-saturate mineral assemblages immediately below the wet solidus, yet have the system go fluid absent on the formation of a very low proportion melt evolved at the wet granite solidus. At the proposed PT conditions of melting for the CGS S-type granites (close to 850°C and 10 kbar) these proportions are 40 wt% leucogranitic melt coexisting with 60 wt% solid phases, with the latter comprising biotite, quartz, plagioclase and garnet in the proportions 10:31:29:30 (Table 2). These proportions are consistent with a large body of experiments on the melting of metapelites and metapsammites at 10 kbar (Patino-Douce 1996; Montel and Vielzeuf 1997; Stevens et al. 1997). Quartz, plagioclase and biotite are reactant phases which, under these conditions, persist in the source composition. Calculated melt and garnet compositions at 850°C and 10 kbar (similar to experimental compositions used by Stevens et al. 2007) are presented in Table 1 from the same pseudosection used to determine phase proportions.

Trace element equilibrium melting

The TEEM composition is generated by assuming that melting and melt extraction occur over a time period long enough such that zircon and monazite are allowed to dissolve in the melt until saturation is reached, or until the accessory phase is exhausted in the source. The composition is calculated using the BS4 source composition (Table 1); the mineral proportions from the pseudosection as determined above; a self-consistent set of partition coefficients ($Kd_n^i = \frac{C_n^i}{C_l^i}$ where C_s^i is the concentration of the element i in the mineral n and C_l^i the concentration of i in the melt) from Montel (1996; Table 1); and a batch melting equation (Eq. 1).

$$C_l^i = \frac{C_0^i}{[F + D^i \times (1 - F)]} \quad \text{and} \quad D^i = \sum_n \left(x_n \times Kd_n^i\right) \tag{1}$$

In Eq. 1, C_l^i is the concentration of i in the resulting melt and C_0^i the concentration of the element i in the source. F is the melt fraction, D^i is the distribution coefficient of the element i in the solid fraction of the partial melting reaction. Kd_n^i is the partition coefficient of i in mineral n, and x_n the proportion of mineral n. Zircon and monazite dissolution is controlled by Zr and LREE saturation, respectively, and can be determined from the major element composition of the melt and the saturation equations of Montel (1993) and Watson and Harrison (1983) at the temperature of partial melting (i.e. 850°C). The composition of the melt is expressed using the variable FM (Eq. 2, molar concentrations), defined as:

$$FM = \frac{\mathrm{Na} + \mathrm{K} + 2 \times (\mathrm{Ca} + \mathrm{Fe} + \mathrm{Mg})}{\mathrm{Al} \times \mathrm{Si}} \tag{2}$$

The variable FM is preferred to the M parameter used by Watson and Harrison (1983), as it produces a better fit with natural rock data, as discussed in Baker et al. (2002) and Kelsey et al. (2008). Zircon and monazite saturation levels are calculated using the equations of Watson and Harrison (1983) and Montel (1993) modified from Baker et al. (2002) and Kelsey et al. (2008); Eqs. 3 and 4, respectively.

$$\ln\left(\frac{\mathrm{Zr}_{\mathrm{zircon}}}{\mathrm{Zr}_{\mathrm{melt}}}\right) = \frac{11,574}{T} - 0.679 \times FM - 1.7965 \tag{3}$$

$$\ln\left(\frac{\mathrm{LREE}_{\mathrm{monazite}}}{\mathrm{LREE}_{\mathrm{melt}}}\right) = -\frac{310}{T} - 1.324 \times FM - 7.5852 \tag{4}$$

where LREE = La + Ce + Pr + Nd + Sm + Gd.

At 850°C, the melt Zr saturation level is 199 ppm, whilst monazite saturation is reached at a total LREE concentration of 1,224 ppm. For the combination of melt proportion and melt and source rock compositions used in this study, monazite saturation is never attained (i.e. all of the monazite can dissolve in the melt). In contrast, zirconium saturation in the melt is readily achievable, with a significant fraction of zircon remaining undissolved. This indicates further that the source composition used in the modelling is potentially realistic as it is consistent with the general lack of observed monazite inheritance and the common observed zircon inheritance in S-type granites.

As the melt and peritectic phases form concurrently, the trace element composition of the peritectic phases is calculated as being in equilibrium with the melt, as predicted by the relevant Kd^i. As a consequence, the trace element composition of the melt produced in the TEEM scenario is rich in LREE due to monazite dissolution (Ce = 108 ppm). However, the HREE contents are relatively low because the HREE liberated by substantial zircon dissolution are largely partitioned into the peritectic garnet. Thus, the Yb concentration in TEEM melt composition is only 0.5 ppm and that

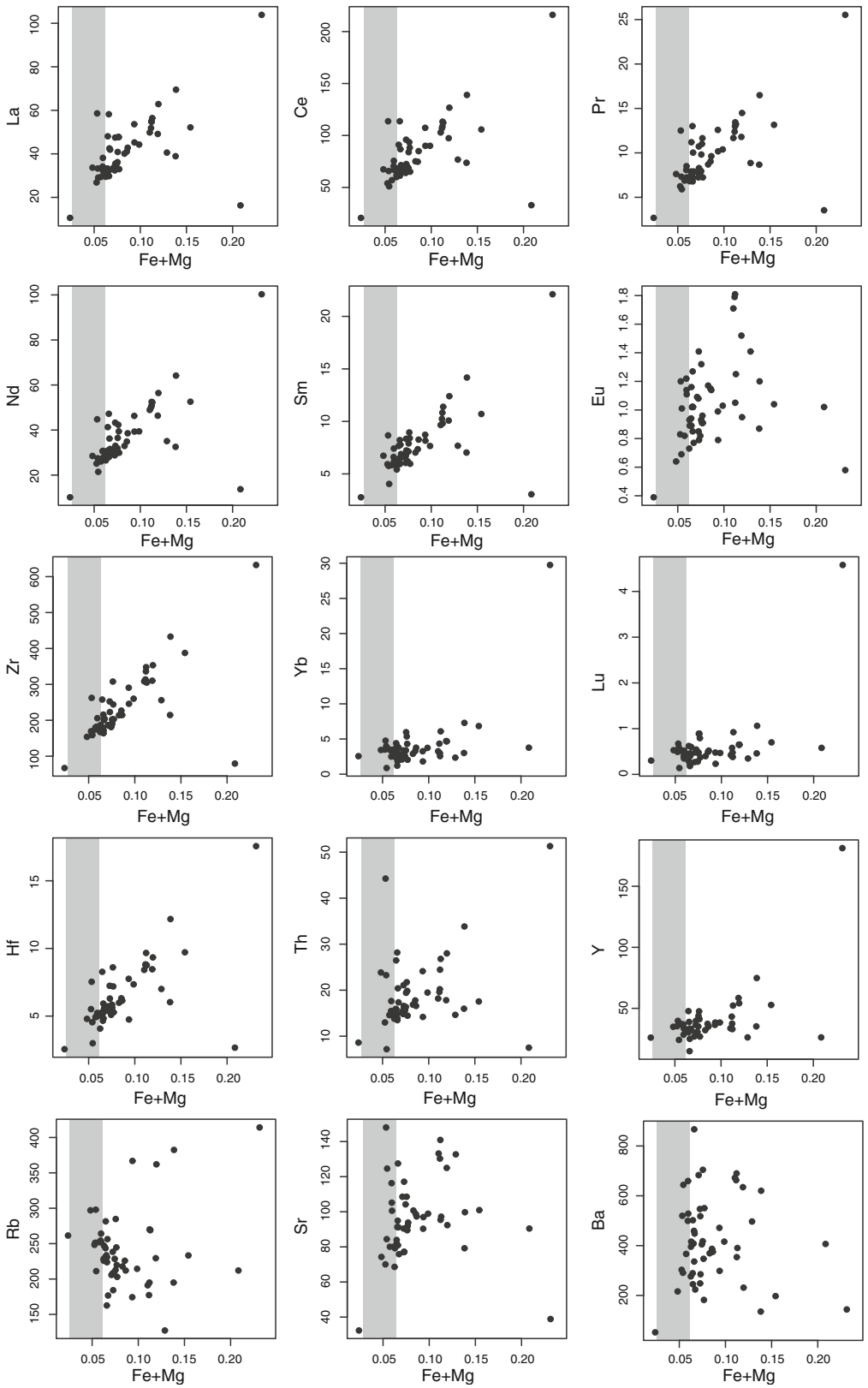

Fig. 5 Trace element versus Fe + Mg variation diagrams for the Peninsular Pluton. *Grey shaded areas* represent Fe + Mg range in experimental melt composition (as in Fig. 4)

Table 1 Trace element composition of monazite (mnz) and zircon (zrc); major and trace element of the source and the calculated zircon-and-monazite-free source

	zrc	mnz	Meta-sedimentary source	Zircon- and monazite-free source
SiO_2	–	–	65.5	
TiO_2	–	–	0.8	
Al_2O_3	–	–	15.0	
FEOt	–	–	5.3	
MnO	–	–	0.1	
MgO	–	–	3.1	
CaO	–	–	1.5	
Na_2O	–	–	2.7	
K_2O	–	–	3.4	
Rb	–	–	106	106
Sr	1.4	–	79	79
Hf	10,350	–	9.3	1.6
Zr	461,051	–	348	2.5
Nb	1.75	–	13.5	13.5
Ba	–	–	389	389
La	1.9	147,859	40.6	2.5
Ce	10.1	359,411	83.4	4.1
Nd	7.0	154,036	38.9	13.9
Pr	1.02	375,28	9.7	1.1
Sm	7.1	21,024	7.7	4.2
Eu	0.6	134	1.2	1.1
Gd	34.9	6,569	7.0	6.9
Tb	12.2	314	1.0	0.9
Dy	154	630	6.5	6.2
Ho	55	82	1.3	1.2
Er	244	138	3.8	3.6
Tm	52	11	0.5	0.5
Yb	463	217	3.7	3.3
Y	1,602	1,946	34.3	32.6
Th	96	42,365	13.2	1.3
Eu*/Eu	0.03	0.01	0.16	0.20

of Hf is 11.4 ppm. The relevant calculated melt and mineral compositions are listed in Table 1. The REE patterns in Fig. 6b illustrate the composition of melt and peritectic phases produced during partial melting. These patterns also illustrate the negative Eu anomaly that exists in all the products of the partial melting reaction (Eu/Eu*melt = 0.07 and Eu/Eu*garnet = 0.05), owing to the partitioning of Eu into residual plagioclase.

Trace element disequilibrium melting

In case of TEDM, the trace element composition of the melt is calculated in an identical manner to that described above, but using the modified source composition created by hypothetically removing the trace element contribution of all monazite and zircon from composition BS4. This models the melt composition produced in situations where melting and melt extraction is sufficiently rapid that no significant dissolution of accessory minerals can occur. As is predicted, the melt composition produced from this modified source is strongly depleted in the trace elements hosted in zircon and monazite (Table 1, Fig. 6b). This depletion is particularly marked for the LREE (e.g. La = 1.76 ppm and Ce = 9.09 ppm) as well as Zr and Hf (9 and 7.1 ppm, respectively). The HREE also have particularly low concentrations in the melt (e.g. Yb = 0.2 ppm), as a combination of them being trapped both in zircon and in residual garnet. In general, the melt formed by disequilibrium melting followed by rapid melt segregation from the residuum has lower trace element contents than that formed under the equilibrium case. Concentrations of LREE in the disequilibrium melt are at least ten times lower than in the equilibrium melting case. On the other hand, HREE concentrations are similar to

Table 2 Phase proportions determine at conditions of partial melting (i.e. 850°C and 10 kbar from Villaros et al. 2009) from Perple-X pseudosection calculation using BS4 major element composition in; partition coefficients (Kd's) from Montel (1996) are preferred to other Kd's in the literature as they constitute a consistent set for all of the mineral and trace elements of interest in this study

These Kd are similar to those published for smaller sub-sets of minerals and trace elements of interest through natural-rock or experimental studies (Irving and Frey 1978; Nash and Crecraft 1985; Sisson and Bacon 1992; Ewart and Griffin 1994; Streck and Grunder 1997; Rubatto and Hermann 2007)

Mineral modal proportion (%) for partial melting						
Retained from the source		Solid phases				Melt
		60				40
zrc	mnz	bi	pl	q	gt	
0.075	0.028	10	29	31	30	
		Reactants			Products	
Mineral modal proportion (%) in the final magma (after extraction from the source)						
		zrc	mnz	gt	Melt	
	TEDM	0.092	0.034	20	80	
	TEEM	0.041	–			
	Partition coefficient (K_d)					
		bi	pl	q	gt	
	Rb	5	0.1	0.012	0	
	Sr	0.3	12	0.015	0	
	Hf	0.5	0.06	0.018	0.2	
	Zr	0.47	0.1	0.001	0.4	
	Nb	1.3	0.02	0.007	0.1	
	Ba	6	1.5	0.004	0	
	La	0.76	0.3	0.012	0	
	Ce	0.86	0.21	0.006	0.1	
	Pr	0.07	4.22	0.001	0.9	
	Nd	0.9	0.14	0.009	0.4	
	Sm	1	0.11	0.008	0.9	
	Eu	0.59	5	0.03	1.2	
	Gd	0.6	0.1	0.007	4	
	Tb	0.87	0.09	0.007	9	
	Dy	0.5	0.07	0.01	26	
	Ho	0.16	1	0.01	32	
	Er	0.41	0.06	0.011	38	
	Tm	0.22	1.63	0.01	45	
	Yb	0.32	0.06	0.012	60	
	Y	1	0.04	0.006	34	
	Th	0.3	0.03	0.006	0.4	

those of the TEEM composition, as they are primarily buffered by garnet, zircon playing a lesser role as even its high Kd's for HREE do not offset the much higher abundance of garnet. LILEs, such as Eu, Rb, Sr or Ba, remain unchanged from the equilibrium case as their concentration in the accessory minerals is very low and their concentration in the melt depends only on the stoichiometry of the partial melting reaction and thus, the proportions of feldspar and biotite consumed. In a similar fashion to melt, peritectic phases in the disequilibrium case are generally depleted in trace elements compared to the equilibrium case. La and Ce in peritectic garnet have extremely low concentrations (0.04 and 0.91 ppm, respectively) while HREE show similar concentrations compared to the equilibrium case (Yb = 11.94 ppm). Thus, the REE patterns in Fig. 6b for the disequilibrium case show a strong depletion in LREE for melt and peritectic phase. Compare to TEEM case, these compositions are notably different, thus the entrainment of peritectic phase in melt implies different trends particularly marked for LREE compositions, with lower contents LREE in the TEDM than in the TEEM case.

As for TEEM, the products of partial melting also show a negative Eu anomaly (Eu/Eu*melt = 0.082 and Eu/Eu*garnet = 0.047) inherited from the source composition and enhanced by the plagioclase-bearing residue. The white star in Fig. 7 illustrates the melt composition produced by TEDM case, while the grey star illustrates the melt composition produced by the TEEM case.

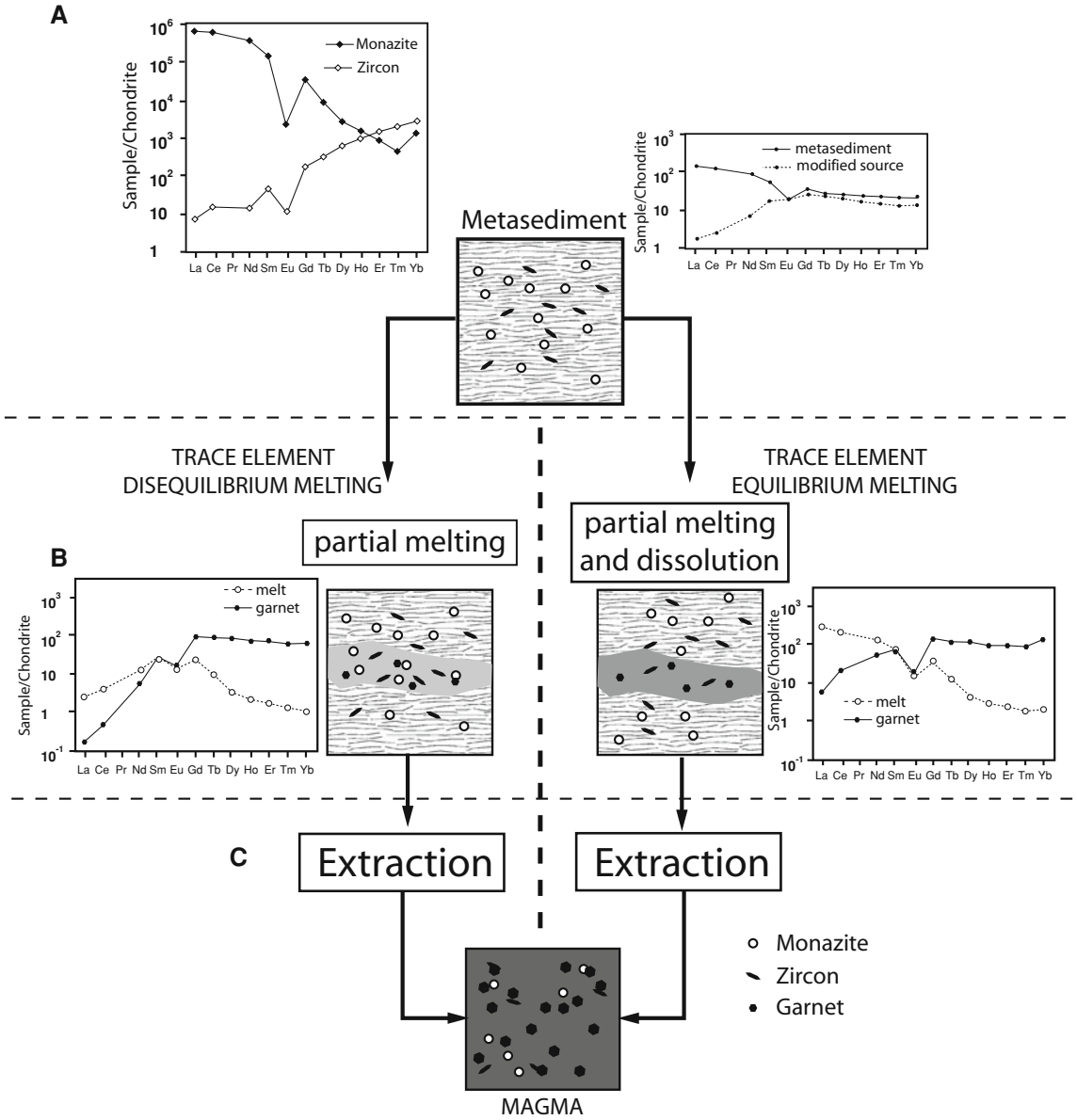

Fig. 6 A diagrammatic illustration of the principles underpinning the trace element modelling in this study. The trace element data are chondrite normalised (from Taylor and McLennan 1985). The top, **a** represents the metasedimentary source including the accessory minerals zircon and monazite. The plot to the left in **a** represents the composition of the accessory minerals. The plot to the right indicates the composition of the original metasediment (top line) and the effective composition of the source composition assuming that none of the accessory minerals are available for reaction (lower line). In the middle, **b** the two end-member cases for behaviour during partial melting in the source are illustrated. In the situation depicted in the pair of diagrams to the left, melting occurs without the dissolution of any accessory phases in the melt, although peritectic minerals are entrained. In this case, the segregated magma contains peritectic phases and accessory minerals and the trace element budget of the magma is solely a function of the proportion of accessory minerals entrained. The pair of diagrams to the right illustrates the opposite scenario. Accessory minerals dissolve in the melt, until the elements that control accessory mineral stability (e.g. Zr in the case of zircon) are saturated in the melt. **c** represents the result, which in terms of concentrations can be identical. However, the path to the right will always produce trace element concentrations no lower than zircon and monazite saturation or than the complete dissolution of these phases in the source will produce, depending on the source composition relative to the saturation concentrations of the relevant elements in the melt at the conditions of anatexis. The path to the left will be characterised by trace element concentrations that can be as low as those of the pure melt that has not dissolved and zircon or monazite

Modelling phase entrainment

The consequences of the entrainment of both peritectic phases and accessory minerals for the magma composition can be modelled using each of the two melt and two garnet (i.e. in TEEM and TEDM cases) compositions described above. The peritectic assemblage of garnet and ilmenite has been added to each of the melt compositions in five

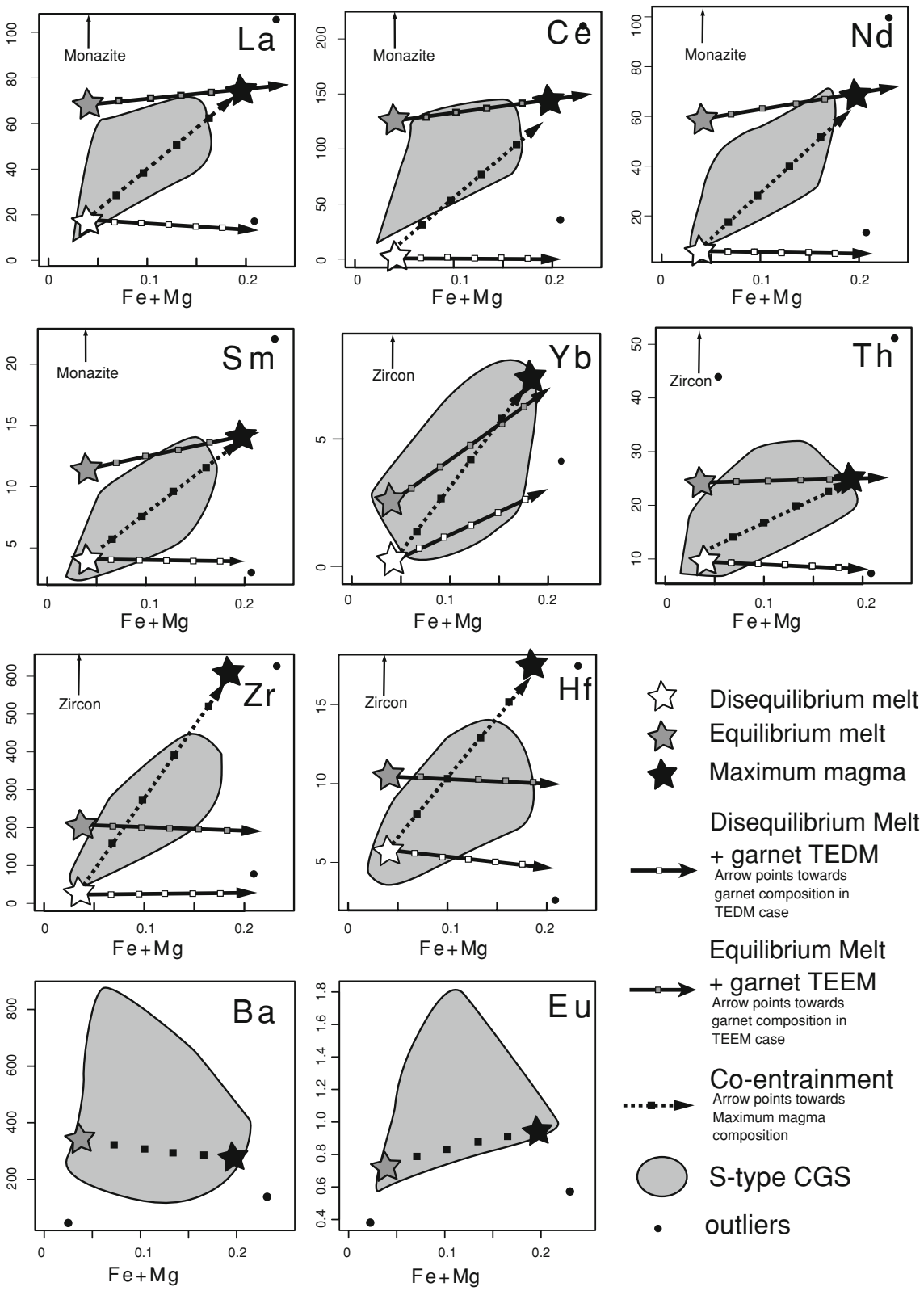

Fig. 7 Results of modelling compared to compositions of the S-type CGS described in Table S1. Diagrams show the variations of trace element concentrations versus atomic Fe + Mg. "Maximum magma" is the addition of the totality of accessory minerals available, 20% of peritectic garnet to melt composition. Co-entrainment trend is an examples leading to the "maximum" composition of magma

increments of 4 wt%. As illustrated by Stevens et al. (2007), this produces the range of major element compositions exhibited by the Peninsular Pluton, from leucogranitic (pure melt) melt to the most FeO + MgO-rich granodiorite (melt plus 20 wt% peritectic assemblage). The vectors of compositional evolution away from the leucocratic model melt compositions that arise as a result of this are illustrated in Fig. 7.

As illustrated in Fig. 1, Zr in granites shows a positive correlation with maficity and in individual suites such as the CGS Zr commonly correlates quite tightly with maficity. Thus, if maficity is a function of peritectic phase entrainment, then co-entrainment of accessory and peritectic minerals commonly occurs. It is perhaps predictable that these functions are coupled, as circumstances that favour the entrainment of a greater proportion of peritectic phases may also favour the entrainment of more of the available accessory minerals. This coupled peritectic assemblage-accessory mineral co-entrainment has been modelled by allowing the entrainment of all of the available accessory minerals. As stated above, the amount of accessory minerals represents 0.075 wt% zircon and 0.028 wt% monazite in the source. After melt extraction, the maximum proportions of remaining minerals (i.e. not dissolved) in the resulting magma are 0.034 wt% monazite and 0.092 wt% zircon of the final magma in the TEDM case and only 0.041 wt% zircon in the TEEM (as all monazite is dissolved in the melt), concurrently with the maximum amount of peritectic phase entrainment (20 wt%). Thus, in modelling peritectic assemblage and accessory mineral co-entrainment, each 4 wt% increment of peritectic assemblage addition also involves the incorporation of 20% of the available accessory mineral assemblage. On Fig. 7 the resultant lines of compositional evolution for the magma follow the dashed arrows.

Results and discussion

Calculated melt compositions compared to the granites

For the trace elements contained within monazite and zircon, the lowest trace element concentrations recorded in the Peninsular Pluton are an identical to, or a very close match with, the modelled TEDM compositions. These compositions are recorded in the most leucocratic rocks, i.e. those compositions proposed by Stevens et al (2007) to most closely match pure melts. Within this least mafic portion of the population, elements that are markers for the behaviour of zircon (mainly Hf and Zr) have values significantly below melt saturation values. In contrast, the highest concentrations of these elements are recorded in the most mafic portions of the granite. In a significant fraction of these most mafic rocks, Zr exceeds saturation values by a considerable margin (Fig. 7), consistent with the common xenocrystic zircons (e.g. Bea et al. 2007) in these rocks. Elements that reflect monazite behaviour (La, Ce, Pr, Sm, Nd and Th) show similar characteristics, with the concentrations of these elements closely matching the predicted TEDM compositions in the most leucocratic granites. In the most mafic granites, these elements are very close to saturation values, but generally do not exceed these limits. On plots comparing trace element concentration to maficity, much of the Peninsular Pluton dataset populates the compositional space located between the TEDM and the magma arising as mixtures of the TEEM, or the TEDM and the peritectic + accessory assemblage, for those elements concentrated in monazite (Fig. 7). Either melt is equally viable in this, as accessory phase dissolution and entrainment are compensatory processes. The elements concentrated in monazite never exceed monazite saturation limits in the magma. This is consistent with the common absence of xenocrystic monazite in S-type granites. It has to be noted that the calculated model matches efficiently the CGS data. Thus it clearly indicates that accessory mineral compositions used for modelling are probably not different than the actual compositions of zircon and monazite entrained in the S-type CGS (Table 3).

On similar plots elements such as Rb, Ba, Sr and Eu show completely different behaviour (Fig. 7). These elements are compatible with reactants of the partial melting reaction and as a result, both our models (TEEM and TEDM) give very similar results; the values resulting from an equilibrium trace element melting model are used here. This may be inappropriate, however, as it assumes equilibration of the residual fraction of these minerals with the melt prior to melt extraction. These elements reach their highest concentrations in granites of intermediate maficity. However, there is a difference in behaviour between elements that follow K and those which follow Ca. Elements such as Ba reach their maximum concentrations towards the more leucocratic side of the major element compositional range (Fig. 7). This is interpreted to reflect source differences, with the most K-rich rocks also being the most Ba-rich and melting to produce melts which leave the source with little entrained peritectic material. In contrast, Eu follows Ca and will partition into residual plagioclase during melting, only becoming liberated as plagioclase becomes exhausted by the melting reaction. Eu concentrations in the source are also likely to be higher in rocks with higher Ca (more plagioclase dominated and/or more calcic plagioclase).

Table 3 Results of calculation

Modelling results					
	Melt		gt		Magma
SiO_2	73.3		39.7		66.5
TiO_2	–		–		–
Al_2O_3	15.0		22.4		16.5
FEOt	0.7		24.1		5.4
MnO	–		0.6		0.1
MgO	0.2		11.5		2.5
CaO	0.6		1.7		0.8
Na_2O	3.1		–		2.5
K_2O	7.1		–		5.7
	TEEM	TEDM	TEEM	TEDM	
Rb	183	183	1.8	1.8	183
Sr	23	23	0.5	0.5	23
Hf	11	7.1	2.3	1.4	21
Zr	200	9.0	80	3.6	622
Nb	6.8	6.8	2.8	2.8	57
Ba	366	367	3.7	3.7	366
La	51	1.8	1.0	0.0	51
Ce	108	9.1	11	0.9	108
Pr	11.2	0.7	10.1	0.7	11.2
Nd	72	42	30	17	72
Sm	13	9	12	8	13
Eu	0.6	0.6	0.8	0.7	0.6
Gd	5.5	5.5	22.1	22.0	5.5
Tb	0.5	0.4	4.2	3.2	0.5
Dy	1.1	0.9	29.8	22.5	1.3
Ho	0.2	0.1	6.0	4.4	0.2
Er	0.5	0.3	18.6	13.0	0.7
Tm	0.1	0.0	2.9	1.8	0.1
Yb	0.5	0.2	27.9	11.9	0.9
Y	4.8	3.5	163	118	6.3
Th	19.6	5.0	8.6	2.2	20
Eu*/Eu	0.07	0.08	0.05	0.05	0.07

TE-DM trace element disequilibrium melting, *TE-EM* trace element equilibrium melting

"Magma" represents the maximum composition calculated here i.e. melt + 20% garnet + all available zircon and monazite

Dissolution of accessory minerals and minimum residence time of melt in the source

A significant fraction of the most leucocratic granites have compositions that indicate that they have escaped their source prior to equilibration with monazite and zircon. In some granites, where zirconium concentrations are below magma saturation levels, the granites do contain xenocrystic zircon. Zircon dissolution rates can be used to constrain the duration of zircon residency in the magma (e.g. Bea et al. 2007). Using a similar approach, the Peninsular Pluton granites with the lowest Zr concentrations can be used to constrain the maximum residence time of the melt in the source, as the source rocks to these granites are very likely to have contained at least some zircon and monazite and the trace element compositions of the rocks may also reflect entrainment of zircon and monazite. To do this, rates of zircon dissolution, as well as zircon abundance and size fraction in the source, need to be known.

The dissolution rate dr/dt (in cm/s) of zircon in peraluminous melt can be determined using Eq. 5 [from Eq. 17 in Watson (1996)]:

$$\frac{dr}{dt} = -(C_{Zr} - C_{Zr*})\left[\left(\frac{1.25 \times 10^{10}}{r}\right) \times e^{\left(-\frac{28,380}{T}\right)} + 7.24 \times 10^{8} \times e^{\left(-\frac{23,280}{T}\right)}\right] \times 10^{-17} \quad (5)$$

where C_{Zr} is the original undersaturated concentration of Zr in the TEDM melt (Zr = 9.0 ppm in the case of these rocks), C_{Zr}* is the saturation concentration of Zr in the melt (i.e. Zr = 199 ppm in the case of these rocks), r is the spherical radius of a hypothetical zircon and T the temperature (in K). Assuming dissolution of spherical zircons in a steady state environment and at constant temperature it is possible to determine the time necessary to reach a given concentration of Zr in the melt.

Figure 8 shows the result of this calculation for three different grain radii: 25, 50 and 75 μm. The minimum Zr content in the S-type CGS recorded in this study is 67.2 ppm. According to Eq. 5 this concentration would be attained in 337 years in the case of 25 μm radius, 1,330 years for 50 μm and finally 3,955 years for 75 μm. As a 75 μm radius would represent an uncommonly large zircon for a metasediment such as BS4, the 3,955 years given by the calculation provides a maximum estimate of the time of residence of melt within the source of the S-type CGS. The estimates of 337–1,330 years obtained for more reasonable size zircons (25 and 50 μm radii, respectively) are much more likely to represent a good bracket for residence time of melt within the source. Using the lower Zr concentration of 9 ppm obtained for TEDM, the dissolution times would be even lower (~30 years for 25 μm radius zircon). Harris et al. (2000) using the same method with a spherical radius of 15 μm and a temperature of 750°C, estimated a residence time of approximately 50 years to model the low Zr concentrations of Himalayan leucogranites. Considering the smaller size of zircons and the lower temperature, these two results agree quite well, and imply relatively a short time of residence of melt in the source of less than 500 years. A further important point to be considered when evaluating the meaning of this value is that the model is built around the incorrect assumption of a static state. Thus,

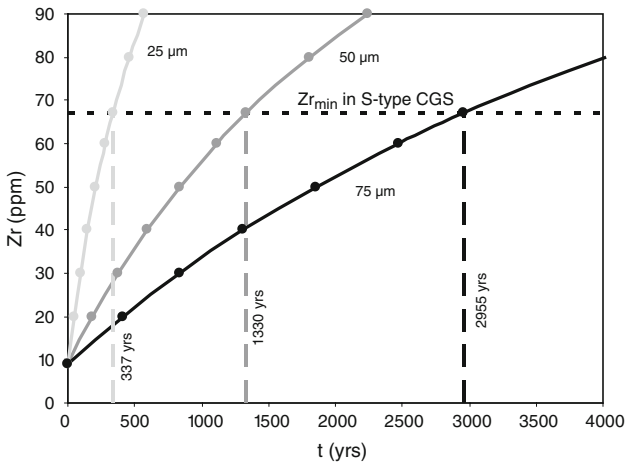

Fig. 8 Zr concentration versus time in a melt. The calculation assume a constant temperature and a complete dissolution of spherical zircons (from Eq. 17 of Watson 1996) Initial zircon radius of 25, 50 and 75 µm and initial undersaturation for Zr of 6.7 ppm (*Black Star*) corresponding to Zr concentration determine for TEDM in Table 1. Zr* is the zirconium saturation at 850°C correspond to Zr concentration in TEEM of Table 1. *Dashed line* indicates temperature at which the minimum undersaturation in the S-type CGS is reached

zircon dissolution is controlled by the diffusion rate of zirconium in the melt and the melt is assumed to be static. Melt flow past the crystal will dramatically reduce the time by replacing Zr-saturated by -undersaturated melt, and melt flow must have occurred as the magma migrated out of the source. Importantly, it is only these leucocratic granites which are least contaminated by entrained phases that provide the possibility to establish this constraint. However, within the Peninsular Pluton there are no intrusive contacts between the various phases of the granite examined in this study. Thus, a very short source residence time is proposed for all of the rocks, with the more trace element enriched granites representing higher levels of entrainment of accessory minerals, not longer source residency times.

Co-entrainment of accessory minerals and peritectic phases

By allowing, for TEDM, rapid melt extraction from the source and coupled accessory mineral and peritectic assemblage entrainment, the model presented here appears to be able to account for the major and trace element geochemistry of the Peninsular Pluton. The reasons for the coupling are probably twofold. First, in high-grade metasediments zircon and monazite commonly occur as inclusions in biotite. Thus, they are liberated by biotite incongruent melting. Secondly, they are liberated in the sites most likely to also be characterised by the growth of peritectic minerals. Thus, physical circumstances favourable to the entrainment of accessory minerals may also act to entrain peritectic crystals. Zircon and monazite are usually present in metasediments as small crystals. Thus, the coupled entrainment described above probably indicates that peritectic crystals entrain as small crystals, possibly with similar grain size distributions to those that characterise the accessory minerals. This process of co-entrainment would appear to not be constrained by degree of melting in the source. Biotite in high grade metasediments very commonly contains inclusions of monazite and zircon. Thus, these minerals are available where melt production is likely to occur. The peritectic minerals form with melt and low melt fractions, if they can efficiently mobilise out of the source, may carry entrained peritectic and accessory phases. At higher melt fractions, the abundance of accessory phases in the source may impinge on the ability of the process to deliver the Zr and LREE enriched compositions displayed by the more mafic granites. However, attaining these melt fractions would require the addition of water to the source and not the fluid absent process, as modelled here, that is commonly considered to account for high level granites (e.g. Stevens and Clemens 1993; Clemens 2006).

Conclusion

Modelling the major and trace element variation in the Peninsular Pluton of the CGS has revealed several important findings. The magmas that intruded at a high level in the crust to build the pluton formed via a TEDM process because the magmas did not spend sufficiently long in the source to establish equilibrium with the relatively refractory zircon and monazite residing there. Maximum magma residence time in the source was less than approximately 500 years and possibly very much less than 500 years, if melt flow and the dynamics of the system are considered. The rocks that appear saturated or close to saturated with regard to zircon and monazite achieved this state not as a result of a Zr or LREE rich melt, but rather by entraining these minerals from the source. In the case of monazite that is very far from saturation, there was sufficient time available in the magmatic environment for monazite equilibration with the melt, as evidenced by its complete dissolution. In the case of zircon, this was not the case as some rocks with zirconium contents lower than saturation values do still contain xenocrystic zircons.

The findings provide very important constraints on the petrogenesis of the different varieties of granite that make up the pluton. Bulk rock compositional ranges such as those in exhibited by the Peninsular Pluton are commonly interpreted to reflect fractional crystallisation (Schoch et al. 1977); or the unmixing of an entrained bulk restite component (Scheepers 1995). The findings of this study prove

that neither process is applicable to these rocks, nor possibly to other S-type rocks, which are all characterised by similar general features. In essence, the leucocratic portions of the pluton have not arisen through fractional crystallisation, or the unmixing of components from a homogenous magma representing more mafic or intermediate granite compositions. These more mafic magmas are typically saturated or close to saturated with regard to zircon and monazite. Consequently, evolution of residual melts via fractionation from these compositions would not be able to form strongly zircon and monazite undersaturated magmas.

Field observations in the Peninsular Pluton allow different phases of the granite to be identified, largely on the basis of different proportions of ferromagnesian minerals. This study shows that variations in major and trace element concentrations were closely correlated. This is interpreted to be a consequence of co-entrainment of peritectic products and accessory minerals from the source. Thus, the magmas which built up the Peninsular Pluton left the source as fundamentally different compositions. These magma batches contributed to pluton growth with sufficiently little mixing that their original chemical character is largely retained.

The fact that well-defined boundaries can be observed between the different Peninsular Pluton phases reflects this lack of mixing. The pluton is reasonably large (at least 40 km in length), yet the boundaries between different facies are generally steeply orientated. As these reflect different discrete magma batches, this orientation would seem to be most consistent with the pluton being fed by a number (perhaps many) smaller conduits, rather than few main feeders from which the pluton inflated. These proposed many conduits would also be consistent with the lack of mixing between magma batches and the tapping of different and discrete magma batches from the source.

Ultimately, this study has demonstrated that it is possible to establish a coherent model for the major and trace element geochemistry of S-type granites.

Acknowledgments The Authors want to thank J. Beard and an anonymous reviewer for their helpful comments that helped improving largely this paper. This work forms part of a PhD study by A. V. A. V. gratefully acknowledges an NRF PhD Bursary and support for the study via National Research Foundation grant funding to G. S. I. S. B. acknowledges support from an Australian Research Council Australian Professorial Fellowship and Discovery Grant No. DP0342473.

References

Ayres M, Harris N (1997) REE fractionation and Nd-isotope disequilibrium during crustal anatexis: constraints from himalayan leucogranites. Chem Geol 139:249–269. doi:10.1016/S0009-2541(97)00038-7

Baker DR, Conte AM, Freda C, Ottolini L (2002) The effect of halogens on Zr diffusion and zircon dissolution in hydrous metaluminous granitic melts. Contrib Mineral Petrol 142:666–678

Bea F (1996a) Residence of REE, Y, Th and U in granites and crustal protoliths: implications for the chemistry of crustal melts. J Petrol 37:521–552. doi:10.1093/petrology/37.3.521

Bea F (1996b) Controls on the trace element composition of crustal melts. Trans R Soc Edinb Earth Sci 87:33–41

Bea F, Montero P, Ortega M (2006) A LA-ICP-MS evaluation of Zr reservoirs in common crustal rocks: implications for Zr and Hf geochemistry, and zircon-forming processes. Can Mineral 44:693–714. doi:10.2113/gscanmin.44.3.693

Bea F, Montero P, Gonzalez-Lodeiro F, Talavera C (2007) Zircon inheritance reveals exceptionally fast crustal magma generation processes in central Iberia during the Cambro-Ordovician. J Petrol 48:2327–2339. doi:10.1093/petrology/egm061

Bhadra S, Das S, Bhattacharya A (2007) Shear zone-hosted migmatites (Eastern India): the role of dynamic melting in the generation of REE-depleted felsic melts, and implications for disequilibrium melting. J Petrol 48:435–457. doi:10.1093/petrology/egl066

Chappell BW (1984) Source rocks of I- and S-type granites in the Lachlan Fold Belt, southeastern Australia. Philos Trans R Soc Lond A 310:693–707

Chappell BW, White AJR (1974) Two contracting granite types. Pac Geol 8:173–174

Chappell BW, White AJR (1992) I-type and S-type granites in the Lachlan fold belt. Trans R Soc Edinb Earth Sci 83:1–26

Clemens JD (2003) S-type granitic magmas—petrogenetic issues, models and evidence. Earth Sci Rev 61:1–18. doi:10.1016/S0012-8252(02)00107-1

Clemens JD (2006) Melting of the continental crust: fluid regimes, melting reactions and source-rock fertility. In: Brown M, Rushmer T (eds) Evolution and differentiation of the continental crust. Cambridge University Press, UK, pp 297–331

Clemens JD, Droop GTR, Stevens G (1997) High-grade metamorphism, dehydrations and crustal melting: a reinvestigation based on new experiments in the silica-saturated portion of the system KAlO2-MgO-SiO2-H2O-CO2 at P $\leq$ 1.5 GPa. Contrib Mineral Petrol 129:308–325. doi:10.1007/s004100050339

Collins WJ, Hobbs BE (2001) What caused the early Silurian change from mafic to silicic (S-type) magmatism in the eastern Lachlan Fold Belt? Aust J Earth Sci 48:25–41. doi:10.1046/j.1440-0952.2001.00837.x

Connolly JAD (1990) Multivariable phase diagrams: an algorithm based on generalized thermodynamics. Am J Sci 290:666–718

Connolly JAD, Petrini K (2002) An automated strategy for calculation of phase diagram sections and retrieval of rock properties as a function of physical conditions. J Metab Geol 20:697–708. doi:10.1046/j.1525-1314.2002.00398.x

Copeland P, Parrish RR, Harrison TM (1988) Identification of inherited radiogenic Pb in monazite and its implications for U-Pb systematics. Nature 333:760–763. doi:10.1038/333760a0

Da Silva LC, Gresse PG, Scheepers R, McNaughton NJ, Hartmann LA, Fletcher I (2000) U-Pb SHRIMP and Sm-Nd age constraints on the timing and sources ot the Pan-African Cape Granite Suite, South Africa. J Afr Earth Sci 30:795–815. doi:10.1016/S0899-5362(00)00053-1

Da Silva LC, McNaughton NJ, Armstrong RA, Hartmann LA, Fletcher IR (2005) The Neoproterozoic Mantiqueira Province and its African connection: a zircon based U-Pb geochronologic subdivision for the Brasiliano/Pan-African systems of orogens. Precambrian Res 136:203–240. doi:10.1016/j.precamres.2004.10.004

Downes H, Dupuy C, Leyreloup A (1990) Crustal evolution of the Hercynian belt of Western Europe: evidence from lower crustal xenoliths (French Massif Central). Chem Geol 83:209–231. doi:10.1016/0009-2541(90)90281-B

Eggins S (2003) Laser ablation ICP-MS analysis of geological materials prepared as lithium borate glasses. Geostand Geoanal Res 27:147–162. doi:10.1111/j.1751-908X.2003.tb00642.x

Elburg MA (1996) U-Pb ages and morphologies of zircon in micrograniteoid enclaves and peraluminous host granite: evidence for magma mingling. Contrib Mineral Petrol 123:177–189. doi:10.1007/s004100050149

Ewart A, Griffin WL (1994) Application of proton-microprobe data to trace-element partitioning in volcanic-rocks. Chem Geol 117:251–284. doi:10.1016/0009-2541(94)90131-7

Gardien V, Thompson AB, Grujic D, Ulmer P (1995) Experimental melting of biotite + plagioclase + quartz ± muscovite assemblages and implications for crustal melting. J Geophys Res Solid Earth 100:15581–15591. doi:10.1029/95JB00916

Georget Y, Martineau F, Capdevila R (1986) Age tardi-hercynien et origine crustale du granite de Brignogan (Finistère, France). Conséquences sur l'interprétation des granites Nord-armoricains = Late-hercynian radiometric age and crustal origin of Brignogan granite (Finistere, France). Consequences on the interpretation of the North-Armorican granites. C R Acad Sci Série 2 Méc Phys Chim Sci Univ Sci Terre 302:237–242

Goad BE, Cerny P (1981) Peraluminous pegmatitic granites and their pegmatite aureoles in the Winnipeg River District, southeastern Manitoba. Can Mineral 19:177–194

Harris N, Ayres M, Massey J (1995) Geochemistry of granitic melts produced during the incongruent melting of muscovite: implications for the extraction of himalayan leucogranite magmas. J Geophys Res 100:15767–15777. doi:10.1029/94JB02623

Harris C, Faure K, Diamond RE, Scheepers R (1997) Oxygen and hydrogen isotope geochemistry of S- and I- type granitoids: the Cape Granite Suite, South Africa. Chem Geol 143:95–114. doi:10.1016/S0009-2541(97)00103-4

Harris N, Vance D, Ayres M (2000) From sediment to granite: timescales of anatexis in the upper crust. Chem Geol 162:155–167. doi:10.1016/S0009-2541(99)00121-7

Hartnady CJH, Newton AR, Theron JN (1974) The stratigraphy and structure of the Malmesbury Group in the southwestern Cape. Bull Precamb Res Unit 15:193–213

Irving AJ, Frey FA (1978) Distribution of trace-elements between garnet megacrysts and host volcanic liquids of kimberlitic to rhyolitic composition. Geochim Cosmochim Acta 42:771–787. doi:10.1016/0016-7037(78)90092-3

Johannes W, Ehlers C, Kriegsman LM, Mengel K (2003) The link between migmatites and S-type granites in the Turku area, southern Finland. Lithos 68:69–90. doi:10.1016/S0024-4937(03)00032-X

Jung S, Mezger K, Masberg P, Hoffer E, Hoernes S (1998) Petrology of an intrusion-related high-grade migmatite: implications for partial melting of metasedimentary rocks and leucosome-forming processes. J Metab Geol 16:425–445. doi:10.1111/j.1525-1314.1998.00146.x

Kelsey DE, Clark C, Hand M (2008) Thermobarometric modelling of zircon and monazite growth in melt-bearing systems: examples using model metapelitic and metapsammitic granulites. J Metab Geol 26:199–212. doi:10.1111/j.1525-1314.2007.00757.x

Kingsbury JA, Miller CF, Wooden JL, Harrison TM (1993) Monazite paragenesis and U–Pb systematics in rocks of the eastern Mojave Desert, California: implications for thermochronometry. Chem Geol 110:147–168. doi:10.1016/0009-2541(93)90251-D

Montel J-M (1993) A model for monazite melt equilibrium and application to the generation of granitic magmas. Chem Geol 110:127–146. doi:10.1016/0009-2541(93)90250-M

Montel JM (1996) Géochimie de la fusion de la croûte continentale. University of Blaise Pascal, Clermont-Ferrand

Montel JM, Vielzeuf D (1997) Partial melting of metagreywackes. 2. Compositions of minerals and melts. Contrib Mineral Petrol 128:176–196. doi:10.1007/s004100050302

Nabelek PI, Glascock MD (1995) Rare earth element-depleted leucogranites Black Hills, South Dakota: a consequence of disequilibrium melting of monazite-bearing schists. J Petrol 36:1055–1071

Nash WP, Crecraft HR (1985) Partition coefficients for trace elements in silicic magmas. Geochim Cosmochim Acta 49:2309–2322. doi:10.1016/0016-7037(85)90231-5

Parrish RR (1990) U-Pb dating of monazite and its application to geological problems. Can J Earth Sci 27:1431–1450

Patino-Douce AE (1996) Effect of pressure and H_2O content on the compositions of primary crustal melts. Trans R Soc Edinb Earth Sci 87:11–21

Patino-Douce AE, Beard JS (1995) Dehydration-melting of biotite gneiss and quartz amphibolite from 3 to 15 Kbar. J Petrol 36:707–738

Patino-Douce AE, Harris N (1998) Experimental constrains on Himalayan anatexis. J Petrol 39:689–710. doi:10.1093/petrology/39.4.689

Patino-Douce AE, Johnston AD (1991) Phase equilibria and melt productivity in the pelitic system: implications for the origin of peraluminous granitoids and aluminous granulites. Contrib Mineral Petrol 107:202–218. doi:10.1007/BF00310707

Pearce NJG, Perkins WT, Westgate JA, Gorton MP, Jackson SE, Meal CR, Chenery SP (1997) A compilation of new and published major and trace element data for NIST SRM 610 and NIST SRM 612 glass reference materials. Geostand Newsl 21:115–144. doi:10.1111/j.1751-908X.1997.tb00538.x

Pickering JM, Johnston AD (1998) Fluid-absent melting behaviour of a two-mica metapelite: experimental constraints on the origin of black hills granite. J Petrol 39(10):1787–1804. doi:10.1093/petrology/39.10.1787

Rollinson H (1993) Using geochemical data: evaluation, presentation, interpretation. Edinburgh Gate, Edinburgh

Rozendaal A, Gresse PG, Scheepers R, Le Roux JP (1999) Neoproterozoic to early Cambrian crustal evolution of the Pan-African Saldania Belt, South Africa. Precambrian Res 97:303–323. doi:10.1016/S0301-9268(99)00036-4

Rubatto D, Hermann J (2007) Experimental zircon/melt and zircon/garnet trace element partitioning and implications for the geochronology of crustal rocks. Chem Geol 241:38–61. doi:10.1016/j.chemgeo.2007.01.027

Sawyer EW (1991) Disequilibrium melting and the rate of melt residuum separation during migmatization of mafic rocks from the Grenville Front, Quebec. J Petrol 32:701–738

Scheepers R (1995) Geology, geochemistry and petrogenesis of Late Precambrian S-, I- and A-type granitoids in the Saldania belt, Western Cape Province South Africa. J Afr Earth Sci 21:35–58. doi:10.1016/0899-5362(95)00087-A

Scheepers R, Armstrong RA (2002) New U-Pb SHRIMP zircon ages of the Cape Granite Suite: implications for the magmatic evolution of the Saldania Belt. S Afr J Geol 105:241–256. doi:10.2113/1050241

Schoch AE (1975) The darling granite batholith. Ann Univ Stell A1:1–104

Schoch AE, Leterrier J, De la Roche H (1977) Major element geochemical trends in the Cape granites. Trans Geol Soc S Afr 80:197–209

Sisson TW, Bacon CR (1992) Garnet high-silica rhyolite trace-element partition-coefficients measured by ion microprobe. Geochim Cosmochim Acta 56:2133–2136. doi:10.1016/0016-7037(92)90336-H

Solgadi F, Moyen J-F, Vanderhaeghe O, Sawyer EW, Reisberg L (2007) The role of crustal anatexis and mantle derived magmas in the genesis of syn-orogenic hercynian granites of the Livradois Area, French Massif Central. Can Mineral 45:581–606. doi:10.2113/gscanmin.45.3.581

Stevens G, Clemens JD (1993) Fluid absent melting and the roles of fluids in the lithosphere: a slanted summary? Chem Geol 108:1–17. doi:10.1016/0009-2541(93)90314-9

Stevens G, Clemens JD, Droop GTR (1997) Melt production during granulite-facies anatexis: experimental data from primitive metasedimentary protoliths. Contrib Mineral Petrol 128:352–370. doi:10.1007/s004100050314

Stevens G, Villaros A, Moyen JF (2007) Selective peritectic garnet entrainment as the origin of geochemical diversity in S-type granites. Geology 35:9–12. doi:10.1130/G22959A.1

Streck MJ, Grunder AL (1997) Compositional gradients and gaps in high-silica rhyolites of the Rattlesnake Tuff, Oregon. J Petrol 38:133–163. doi:10.1093/petrology/38.1.133

Sylvester P (1998) Post-collisional strongly peraluminous granites. Lithos 45:29–44. doi:10.1016/S0024-4937(98)00024-3

Taylor SR, McLennan SM (1985) The continental crust: its composition and evolution. Blackwell, New York

Vielzeuf D, Holloway JR (1988) Experimental determination of fluid absent melting relations in the pelitic system. Contrib Mineral Petrol 98:257–276. doi:10.1007/BF00375178

Vielzeuf D, Montel JM (1994) Partial melting of Metagreywackes. 1. Fluid-absent experiments and phase-relationships. Contrib Mineral Petrol 117:375–393. doi:10.1007/BF00307272

Villaros A, Stevens G, Buick IS (2009) Tracking S-type granite from source to emplacement: clues from garnet in the Cape Granite Suite. Lithos (in press)

Villaseca C, Orejana D, Paterson BA (2007) Zr–LREE rich minerals in residual peraluminous granulites, another factor in the origin of low Zr–LREE granitic melts? Lithos 96:375–386. doi:10.1016/j.lithos.2006.11.002

Watson EB (1996) Dissolution, growth and survival of zircons during crustal fusion: kinetic principles, geological models and implications for isotopic inheritance. Trans R Soc Edinb Earth Sci 87:43–56

Watson EB, Harrison TM (1983) Zircon saturation revisited—temperature and composition effects in a variety of crustal magma types. Earth Planet Sci Lett 64:295–304. doi:10.1016/0012-821X(83)90211-X

Watt GR, Harley SL (1993) Accessory mineral phase controls on the geochemistry of crustal melts and restites produced during water-undersaturated partial melting. Contrib Mineral Petrol 114:550–566. doi:10.1007/BF00321759

White AJR, Chappell BW (1977) Ultrametamorphism and granitoid genesis. Tectonophysics 43:7–22. doi:10.1016/0040-1951(77)90003-8

Williamson BJ, Shaw A, Downes H, Thirlwall MF (1996) Geochemical constraints on the genesis of hercynian two-mica leucogranites from the Massif Central, France. Chem Geol 127:25–42. doi:10.1016/0009-2541(95)00105-0

Williamson BJ, Downes H, Thirlwall MF, Beard A (1997) Geochemical constraints on restite composition and unmixing in the Velay anatectic granite, French Massif Central. Lithos 40:295–319. doi:10.1016/S0024-4937(97)00033-9